Available online at www.sciencedirect.com

SCIENCE DIRECT®

Tectonophysics 398 (2005) 101–114

TECTONOPHYSICS

www.elsevier.com/locate/tecto

Relocated aftershocks of the March 10, 1988 Trinidad earthquake: Normal faulting, slab detachment and extension at upper mantle depths

J.L. Marshall, R.M. Russo*

Department of Geological Sciences, Northwestern University, Evanston, IL 60208, USA

Received 26 January 2004; accepted 29 November 2004
Available online 5 March 2005

Abstract

We relocated aftershocks of the March 10, 1988 earthquake off the east coast of Trinidad in order to determine the fault plane for the main shock and to understand this anomalous earthquake series. The March 10 main shock (M_W 6.6) was the first significant instrumentally recorded earthquake to occur in the epicentral region east of Trinidad. The reported depth of the main shock, 53 km (by the International Seismological Centre, ISC), is unusual, but is consistent with observations of *pP–P* times. The main shock Harvard centroid moment tensor (CMT) solution, nearly pure normal faulting on nodal planes striking ENE, is also unusual given the depths of the seisms and the rarity of extensional faulting at these depths. Using *P* arrival times tabulated by the ISC, we relocated the aftershocks using the joint hypocentral determination method to find new locations relative to the main shock. In map view, the relocated epicenters form a tight elliptical cluster, with major axis trending WNW–ESE and minor axis NNE–SSW. Virtually all the seisms in the earthquake series occurred at depths ranging from 30 to 60 km, deeper than normal crustal earthquakes, in an area previously not considered a locus of subducting lithosphere. The aftershocks define a distinct plane, dipping 34°NW. This dip is consistent with the Harvard CMT focal mechanism of the main shock: one CMT nodal plane dips 38°N and strikes ENE, very close to our estimate of the active fault plane. Thus, the March 10 aftershocks are consistent with slip on the north-dipping plane of the main shock. Because the earthquake series occurred 100 km SE of oceanic South American slab subducting beneath the Caribbean plate, at a depth generally inconsistent with shallow normal faulting outside of slabs, we interpret the main shock as having occurred deep (50 km) in South American lithosphere currently moving NW into the subduction zone. The occurrence of this earthquake indicates an extensional stress applied to the lithosphere of the South American plate, likely related to a combination of slab pull to the NW as the slab subducts beneath the Caribbean plate, and to detachment of the subducting lithosphere from buoyant continental South America.

Keywords: March 10, 1988 Trinidad earthquake; Centroid moment tensor; Aftershocks

* Corresponding author. Now at: Department of Geological Sciences, P.O. Box 112120, University of Florida, Gainesville, FL 32611, USA. Tel.: +1 352 392 6766; fax: +1 352 392 9294.
E-mail address: russo@geology.ufl.edu (R.M. Russo).

0040-1951/$ - see front matter © 2005 Elsevier B.V. All rights reserved.
doi:10.1016/j.tecto.2004.11.010

1. Introduction

The eastern Caribbean (Ca)–South American (SA) plate boundary (Fig. 1) is characterized by dextral transpressional geologic structures, including major right-lateral strike-slip faults and a SE verging fold and thrust belt (Speed, 1985; Rossi et al., 1987; Roure et al., 1994; Parnaud et al., 1995; Passalacqua et al., 1995; Avé Lallement, 1997), and intense shallow (0 to 70 km) and intermediate (>70 km) depth seismicity (Fig. 2; Molnar and Sykes, 1969; Perez and Aggarwal, 1981; Shepherd and Aspinall, 1983; Russo et al., 1992, 1993). The larger magnitude shallow earthquakes in the plate boundary zone are predominantly dextral strike-slip earthquakes on the El Pilar Fault and thrust mechanisms distributed in the wide plate boundary zone, although a few normal faulting events are known (Rial, 1978; Russo et al., 1992, 1993). The geology and seismicity patterns are generally consistent with geodetically observed dextral motion between the Caribbean and South American plates (Weber et al., 2001; Perez et al., 2001). South American Atlantic oceanic lithosphere subducts with attendant seismic activity beneath the Caribbean plate along the Lesser Antilles island arc (Molnar and Sykes, 1969; McCann and Sykes, 1984; Stein et al., 1982, 1983; Wadge and Shepherd, 1984; Russo et al., 1992, 1993), and the Lesser Antilles oceanic slab continues aseismically beneath the South American (NE Venezuela) portion of the plate boundary zone, as revealed by tomography and analysis of gravity anomalies and geology (van der Hilst, 1990; Russo and Speed, 1992, 1994; Russo et al., 1996; VanDecar et al., 2003).

The March 10, 1988, magnitude 6.6 (M_W) earthquake (Figs. 1 and 2) was unusual in its location, depth, focal mechanism and magnitude. This earthquake occurred in a region of little previously recorded seismicity and had an unusual normal faulting focal mechanism (Harvard CMT; Dziewonski et al., 1989), with clear *pP–P* times (Fig. 3) indicating a main shock source depth of around 50 km. The

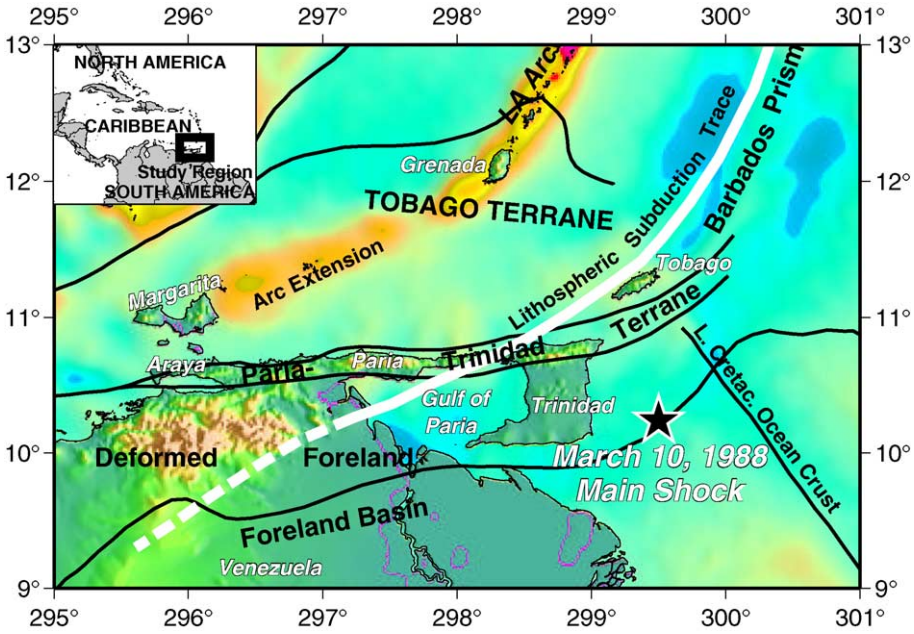

Fig. 1. Geography and major structural boundaries of the study region. Note lithospheric subduction trace (heavy white line), which is the surface projection of the presumed contact between the bottom of Caribbean crystalline lithosphere and subducting South American lithosphere; dashed where slab is detached (Russo et al., 1996; VanDecar et al., 2003). Star is location of March 10, 1988 main shock. Land masses in shaded relief and marine areas show 2-min resolution free-air gravity anomalies of Sandwell and Smith (1997). LA Arc=Lesser Antilles Arc. Note the arc platform extending from Grenada to Margarita is clearly visible in the gravity anomalies (Speed, 1985). This figure can be viewed in colour in the web version of this article.

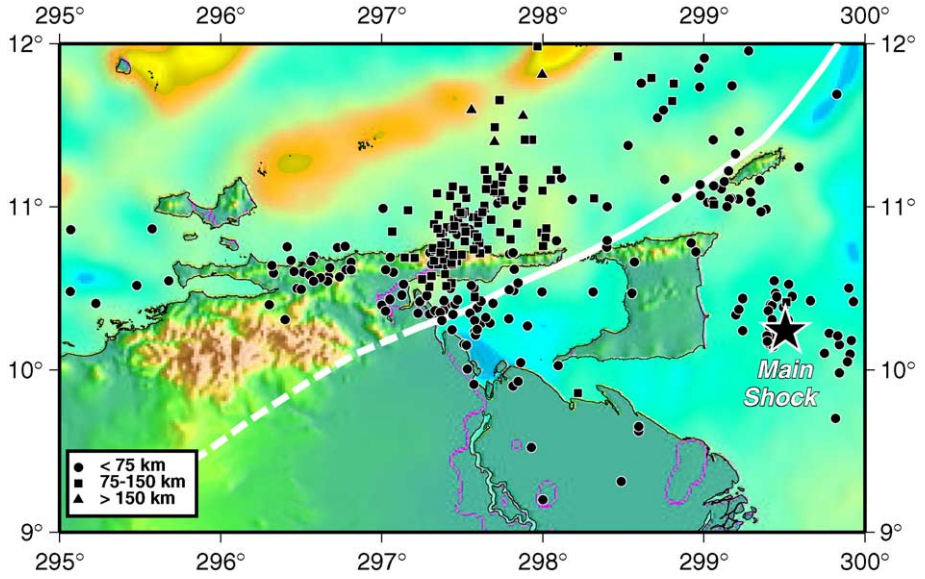

Fig. 2. Seismicity of the study region, 1963–2001 (NEIC). Subducting South American slab is defined seismically along the Lesser Antilles Arc by sporadic seismicity. Note the more frequent earthquakes deeper than 75 km centered around 10.75°N, 297.75°W (Paria Cluster), and the complete absence of this seismicity west of the Gulf of Paria (Perez and Aggarwal, 1981). The March 10, 1988 main shock and aftershocks lie almost 100 km SE of the nearest South American slab subducting beneath Tobago. This figure can be viewed in colour in the web version of this article.

earthquake was followed by many aftershocks, which continued for several years, an unusually long period for an aftershock series. The goal of our study of this earthquake is to determine the active fault plane of the focal mechanism, and thereby to improve our understanding of the region's tectonics.

The main shock occurred about 60 km off the east coast of Trinidad. The main shock epicenter is within the wide eastern Ca–SA plate boundary zone, but the event occurred about 100 km southeast of the boundary between the Caribbean and South American plates, here taken to be the estimated location of the surface projection of the lithospheric subduction trace (slab in contact with the Caribbean mantle, approximately 70 km deep; heavy white line, Figs. 1 and 2) (Russo et al., 1996). The main shock took place within or adjacent to the deformed foreland portion of the Ca–SA plate boundary zone, but its depth, 53 km, is too deep to represent crustal faulting, as expected in this region. The main shock clearly took place in South American continental or transitional lithosphere, as it lies on the continental margin west of the notable join between South American oceanic and continental lithosphere ('Late Cretaceous Ocean Crust' on Fig. 1). This continental lithosphere is within the region of flexural deformation expected as a plate enters a subduction zone; thus, the earthquake could represent flexural deformation deep in the lithosphere. However, extensional deformation related to flexure of the plate should yield very shallow earthquakes with steeply SW-dipping fault planes (e.g., Christmas Day 1969 main shock of Stein et al., 1982), given the steep NW dip of the South American slab to the northwest of the main shock (Perez and Aggarwal, 1981; Russo et al., 1993; VanDecar et al., 2003).

The earthquake series also took place around 100 km east of the current locus of Lesser Antilles slab detachment beneath the Gulf of Paria (Russo et al., 1996; VanDecar et al., 2003). Southwest of the Gulf's western coast, the Lesser Antilles slab is aseismic, detached and lies beneath the Venezuelan Serranía. Directly beneath and NE of the Gulf, the Paria seismic cluster represents the active tearing and detachment of the slab (Russo et al., 1993, 1996). The negative buoyancy pull of the detached portion of the slab (presumably Jurassic age oceanic lithosphere) is transferred to the unsubducted portions of the plate, primarily continental SA lithosphere beneath and east of Trinidad (Russo et al., 1996). Slab detachment

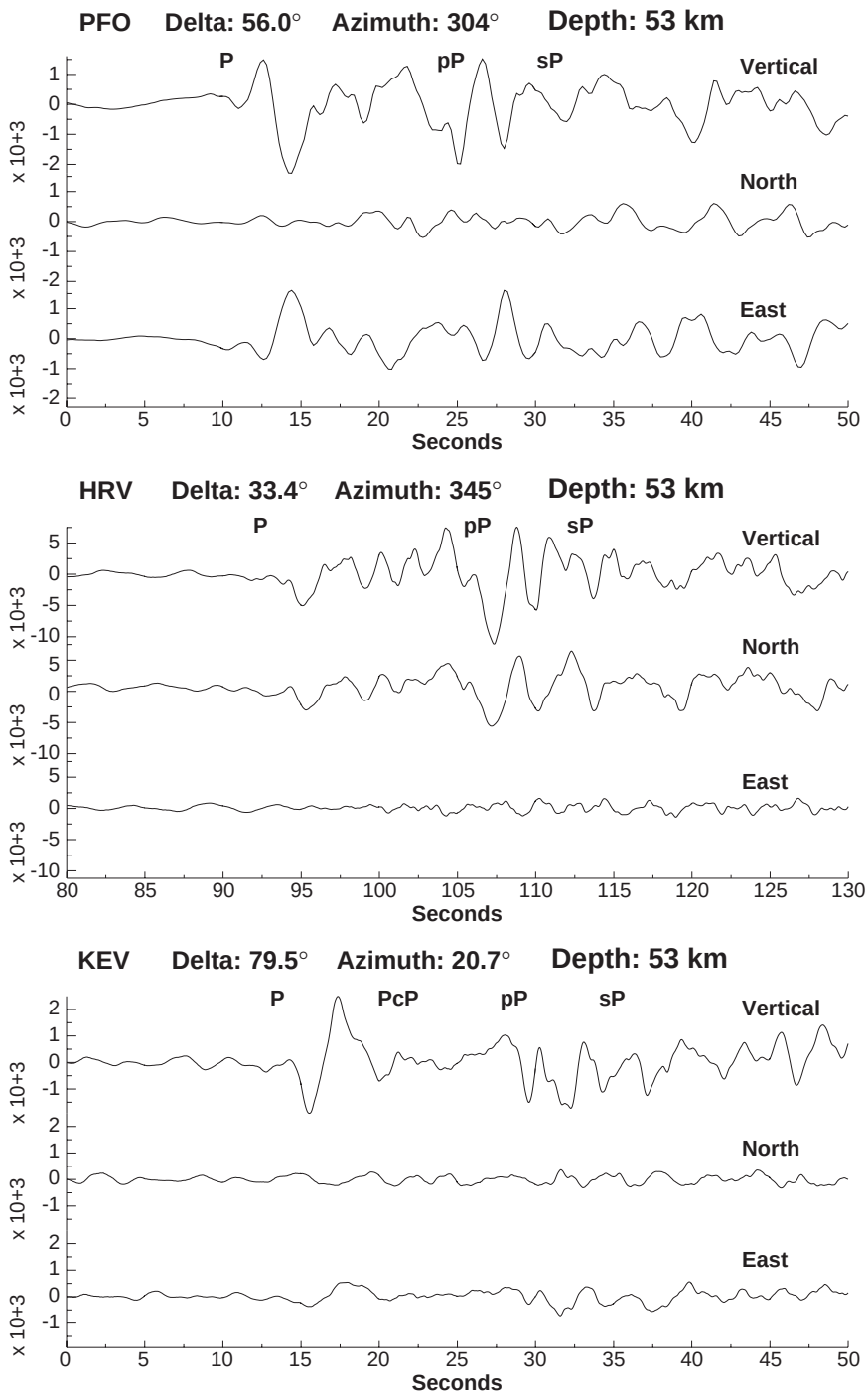

Fig. 3. Seismograms of the first 50 s of the March 10, 1988 earthquake at three teleseismic stations, PFO, HRV and KEV. Estimated arrival times of *P*, *pP* and *sP* calculated for hypocenter depth of 53 km, based on the IASP91 Earth models are shown for each set of seismograms. Note that the phase *pP* is clearly visible on the vertical components. Separation of *P* and *pP* consistent for focal depth around 50 km for arrivals at all three stations.

should result in concentration of slab negative buoyancy stresses around the detachment region, as the weight of the detached portion of the slab is transferred to as yet unsubducted lithosphere (e.g., Wortel and Spakman, 2000). This could enhance slab pull deviatoric stresses and result in extensional earthquakes in the slab at, or updip of, the incipient detachment tear or even in the unsubducted portion of the attached lithosphere. Stresses driving slab detachment are probably also enhanced by the buoyancy of continental South America currently entering the subduction zone in the vicinity of Trinidad and Tobago. Such earthquakes should have active fault planes parallel to local slab strike and dip either towards the subducted slab or approximately perpendicular to the slab face (Yoshioka and Wortel, 1995). Several other normal faulting earthquakes in the Trinidad vicinity are known to have occurred at depths of around 50–60 km, similar to those of the March 10, 1988 main shock (Russo et al., 1992), perhaps delineating the zone of active slab detachment. Note that focal mechanisms resulting from flexural deformation and slab detachment would be identical, the earthquakes differing essentially only in depth (flexural earthquakes expected to be shallow only) if the fault plane is not determined. Fault plane orientation is diagnostic, however, as the flexural events are expected to have fault planes dipping away from the

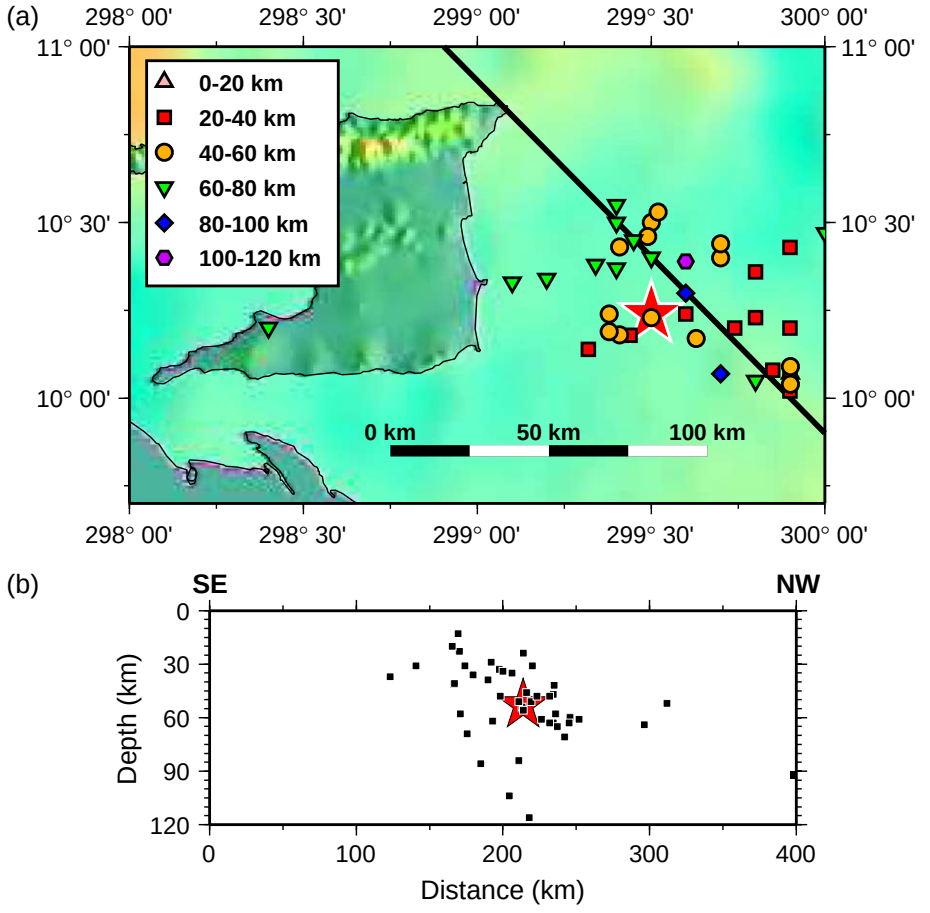

Fig. 4. (a) Map of ISC locations of March 10, 1988 event and aftershocks. Event depths as in key, upper left. (b) Vertical cross sections showing projections of ISC hypocenters onto NW–SE plane (heavy black line on (a)). Note apparently steep northward dip of tabular zone of aftershocks on section. This figure can be viewed in colour in the web version of this article.

subduction trench, thereby allowing plate bending. To assess the applicability of these two possibilities–flexure versus slab detachment–and the different tectonics they represent, we studied the aftershock series of the March 10, 1988 earthquake in order to determine its active fault plane geometry.

2. ISC locations

Aftershocks often occur on or at the boundaries of the region of the fault surface ruptured during large-magnitude earthquakes (e.g., Mendoza and Hartzell, 1988), and thus they can be used to define the active fault plane of a large shock in the absence of independent information like surface rupture (Stein and Barrientos, 1985). The original ISC aftershock locations, when plotted in map view, have an elliptical pattern trending primarily E–W (Fig. 4). This trend is at an angle to both nodal planes of the main shock CMT focal mechanism, and also to the nodal planes of four of the five aftershocks (Fig. 5 and Table 1) large enough to yield focal mechanisms (Dziewonski et al., 1989). The ISC aftershock epicenters are rather spread out, and in cross section yield little information about the possible active fault plane (Fig. 4). On a NW–SE trending vertical section (perpendicular to the strike of the main shock and

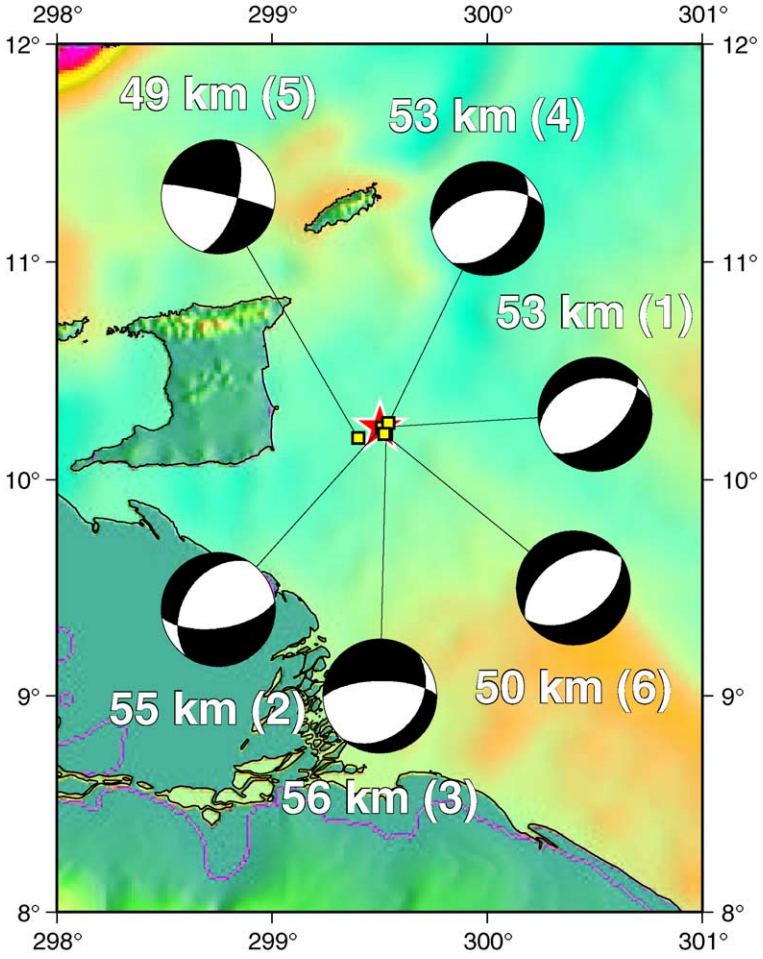

Fig. 5. Focal mechanisms of the March 10, 1988 main shock and five larger magnitude aftershocks. Numbers in parentheses keyed to Table 1. This figure can be viewed in colour in the web version of this article.

Table 1
Focal mechanisms

Event	Date	Origin time	N lat. (°)	W long. (°)	Depth (km)	Strike (°)	Dip (°)	Rake (°)	M_W
1	10 03 88	06:17:17.0	10.24	60.50	53.00	256	38	−67	6.6
2	11 03 88	16:01:02.6	10.24	60.49	55.09	213	38	−132	5.2
3	12 03 88	04:32:05.8	10.21	60.47	56.04	42	31	−133	5.8
4	16 03 88	05:47:58.5	10.26	60.46	53.02	40	45	−118	5.7
5	25 03 88	16:20:42.2	10.19	60.60	48.77	16	63	−174	5.5
6	24 06 88	08:57:49.5	10.21	60.48	50.35	238	44	−89	5.9

large-magnitude aftershock nodal planes), the aftershocks lie in a tabular cluster extending from 10 km to 120 km depth. The vertical section indicates an apparent steep dip to the north, but no clear fault plane defining distribution is apparent, and the aftershock zone delineated by the ISC locations could be vertical, for example. Neither nodal plane of the Harvard CMT focal mechanism matches this aftershock distribution. Also, the apparent extent of the rupture, approaching 110 km in down-dip direction alone as delineated by the ISC locations, is too great to be consistent with the relatively modest magnitude (MW 6.6) of the main shock. For these reasons, it is desirable to restudy the aftershock distribution in order to reconcile them with the main shock focal mechanism and magnitude.

3. Joint hypocenter determination

Analysis of the main shock–aftershock series began with the input of the ISC data of the main shock, in the form of P-wave first arrival times culled from the published ISC Bulletin for March 1988. In order to ensure that we identify and include in our study all possible aftershocks among the totality of seismicity reported to the ISC for the study area, we also input P arrival times for all significant earthquakes from the main shock vicinity that occurred between March 11, 1988 and the end of 1990. We assumed that these events are aftershocks since the area was almost completely devoid of seismicity prior to the main shock, and once relocated those events that were clearly shown not to be true aftershocks of the March 10, 1988 earthquake were dropped from further analysis, although they do appear on maps of the study area. The seismicity, including true aftershocks, were relocated, in two groups (28 and 18 events, respectively) for ease of computation, relative to the main shock location using the joint hypocentral determination (JHD) method of Dewey (1972) (see also Douglas, 1967). Dewey's method assumes that travel time anomalies of *P* waves from the group of earthquakes are identical at all common stations, and thus differences in observed arrival times are due to differences in hypocenter only. A 'master event'–in our case the March 10, 1988 main shock–is assumed to be accurately located, and the parameters sought for each aftershock are essentially the latitude, longitude, depth and origin time differences between the aftershock in question and the main shock. Thus, the method is ideal for our purpose since the location and depth of the main shock are relatively well known and we seek primarily to constrain the fault plane of the main shock, defined by the relative locations of the aftershocks. Solution is by weighted linear least squares, and 90% confidence ellipses are calculated for event latitude, longitude, depth and origin time assuming the travel time errors are normally distributed (Dewey, 1972). P arrivals at 181 stations were used in various combinations for the events of the first group; similarly, P arrivals at 134 stations were used to locate the events of group 2.

The assumption of constant travel time anomalies to common stations is probably not violated for the true aftershocks in our case because of the tight clustering of the main shock and these aftershocks. The few exceptions to this clustering we included in the JHD solution are both irrelevant to our interpretations and serve as a test of the method: events that are true aftershocks should either join or remain in the cluster after JHD, and these are the only events that we wish to influence our interpretation. We argued above that the depth of main shock is probably accurate given the *pP–P* times, but errors in this hypocenter should effect the relative locations of the

aftershocks identically, so the JHD locations should represent the true spatial orientation of the active fault plane. Nonetheless, hypocentral errors should be largest for aftershock depths since the change in travel time with respect to depth is small for shallow earthquakes (Dewey, 1972).

4. Results

The result of relocating the aftershocks is significant (see Table 2). In general, the relocation tended to draw the earthquakes closer together, creating a well-defined epicenter cluster with long axis trending

Table 2
JHD relocations March 10, 1988 event aftershocks

Date	Origin time	Change (s)	N lat. (°)	Change (°)	W long. (°)	Change (°)	Depth (km)	Change (km)
10 03 88	06:17:17.0	0.00	10.24	0.00	60.50	0.00	53.00	0.00
10 03 88	06:30:18.3	−2.70	10.20	−0.03	60.45	0.05	41.02	−12.98
10 03 88	06:33:19.9	−6.30	10.32	−0.18	60.44	0.06	54.48	7.48
10 03 88	23:38:11.5	−4.48	10.36	−0.07	60.15	−0.05	39.10	6.10
11 03 88	00:58:02.0	−4.78	10.48	−0.07	60.55	0.05	59.36	−0.64
11 03 88	06:14:27.5	−4.54	10.47	−0.06	60.35	0.13	51.32	9.32
11 03 88	10:32:32.3	−3.66	10.14	−0.06	60.20	−0.10	43.24	7.24
11 03 88	16:01:02.6	−2.67	10.24	0.06	60.49	0.10	55.09	9.09
12 03 88	04:32:05.8	−4.39	10.21	0.02	60.47	0.15	56.04	5.04
12 03 88	05:24:42.0	−7.01	10.14	−0.26	60.36	0.14	50.05	−10.95
12 03 88	21:37:22.3	−1.27	10.18	0.13	60.43	−0.23	52.92	−16.08
12 03 88	23:00:05.1	−2.89	10.20	−0.03	60.43	−0.23	51.59	12.59
13 03 88	17:00:24.4	0.23	10.28	0.20	60.43	−0.28	51.30	20.30
14 03 88	11:53:32.3	0.30	10.21	0.13	60.44	−0.34	52.24	29.24
16 03 88	05:47:58.5	−4.40	10.26	0.02	60.46	0.16	53.02	5.02
16 03 88	14:24:20.4	−5.59	10.40	−0.06	60.38	0.13	51.41	3.41
17 03 88	11:16:58.2	−6.82	10.27	−0.18	60.49	0.06	55.88	−7.12
18 03 88	03:22:59.1	−2.89	10.38	0.08	60.48	−0.08	60.63	−23.37
20 03 88	00:54:15.3	−3.71	10.36	−0.04	60.47	−0.17	55.67	4.67
24 03 88	14:44:49.0	−3.00	10.50	0.00	60.65	−0.05	57.50	−13.50
25 03 88	16:20:42.2	−1.77	10.19	0.05	60.60	0.08	48.77	17.77
01 04 88	12:59:28.1	−5.64	10.24	−0.10	60.78	0.02	53.01	−9.99
07 04 88	21:47:08.4	−0.59	10.11	0.09	60.37	−0.27	43.93	23.93
14 04 88	07:31:47.9	−1.11	10.51	0.15	60.56	−0.36	52.98	18.98
22 04 88	10:16:17.7	−0.29	10.19	0.15	60.44	−0.34	52.72	11.72
28 04 88	22:15:38.3	−5.72	10.26	−0.11	60.48	0.12	55.87	−7.13
30 04 88	21:37:33.9	−5.13	10.26	−0.14	61.51	0.09	49.74	−2.26
08 05 88	03:15:41.2	−3.79	10.18	−0.06	60.47	−0.07	46.22	11.22
04 06 88	03:29:50.5	−4.54	10.34	−0.10	60.46	−0.16	52.08	−3.92
05 06 88	11:19:24.5	−3.45	11.43	−0.07	59.29	−0.19	108.52	4.52
06 06 88	02:29:08.7	−5.31	10.29	−0.09	60.57	0.09	59.08	−5.92
24 06 88	08:57:49.5	−1.45	10.21	0.03	60.48	0.08	50.35	26.35
24 06 88	10:27:50.3	−2.43	10.36	0.16	61.62	−0.02	23.79	−40.21
24 06 88	10:38:06.0	3.01	10.19	0.29	60.45	−0.55	43.99	12.99
24 06 88	22:25:50.8	−1.16	10.24	0.15	60.40	−0.30	29.18	−28.82
26 06 88	07:03:19.7	−5.42	10.27	−0.16	60.47	0.12	53.84	−4.16
02 09 88	08:30:20.6	−1.39	10.23	0.16	60.49	−0.19	46.11	−39.89
30 10 88	17:25:17.5	0.52	10.25	0.18	60.47	−0.37	40.00	27.00
02 12 88	18:25:16.3	−1.67	10.55	0.22	61.02	−0.12	20.74	−40.26
04 12 88	00:41:00.3	−2.72	10.12	−0.05	60.44	−0.07	45.84	−2.16
03 04 89	01:45:46.5	−4.22	10.67	−0.05	62.37	0.02	67.64	−24.36
15 04 89	14:26:40.3	−3.08	8.58	0.06	60.91	0.15	50.67	13.67
24 09 89	16:56:49.2	−4.84	10.36	−0.11	60.09	−0.09	52.77	−9.23
27 09 89	23:31:29.2	−4.82	10.29	−0.10	60.28	0.12	82.27	−33.73
09 10 90	21:57:16.0	−4.35	10.17	−0.03	60.32	−0.06	41.98	12.98

WNW–ESE about 60 km wide (Fig. 6), indicating that the aftershock cluster dips shallowly to the north. This is visible in the figure via comparison of the locations of aftershocks at 40–50 km (circles) and those at 50–60 km depths (stars): the latter lie almost strictly north of the former, consistent with a northward dip of the earthquake distribution. Although the aftershocks are located deeper than normal crustal thicknesses, from 35–65 km (Fig. 6) with a concentration around 50 km below the surface, the events in the ISC catalogue deeper than 70 km have relocated to shallower depths. In fact, only one aftershock actually has a best-depth estimate deeper than 65 km (Table 2).

On an NW–SE cross section, the relocated aftershocks cluster tightly (Fig. 6), with an apparent deepening northwards, consistent with the inference of northward dip of the aftershock cluster made above. In section, the true aftershocks visibly span a depth range from 35 to 65 km. Given the range of depths and the horizontal area of the aftershock cluster, it is clear that the ruptured fault surface is rather large. The true aftershocks spread over an area that is 30 km in the down dip direction and 80 km along strike.

Relocation vectors (Fig. 7, top) clearly show the tightening of the aftershocks. In particular, the events located furthest to the SE by the ISC are systematically shifted to the NW, into the cluster of events around the main shock epicenter. Northwesterly ISC aftershock epicenters also appear to shift systematically to the SE to overlie the main shock epicenter,

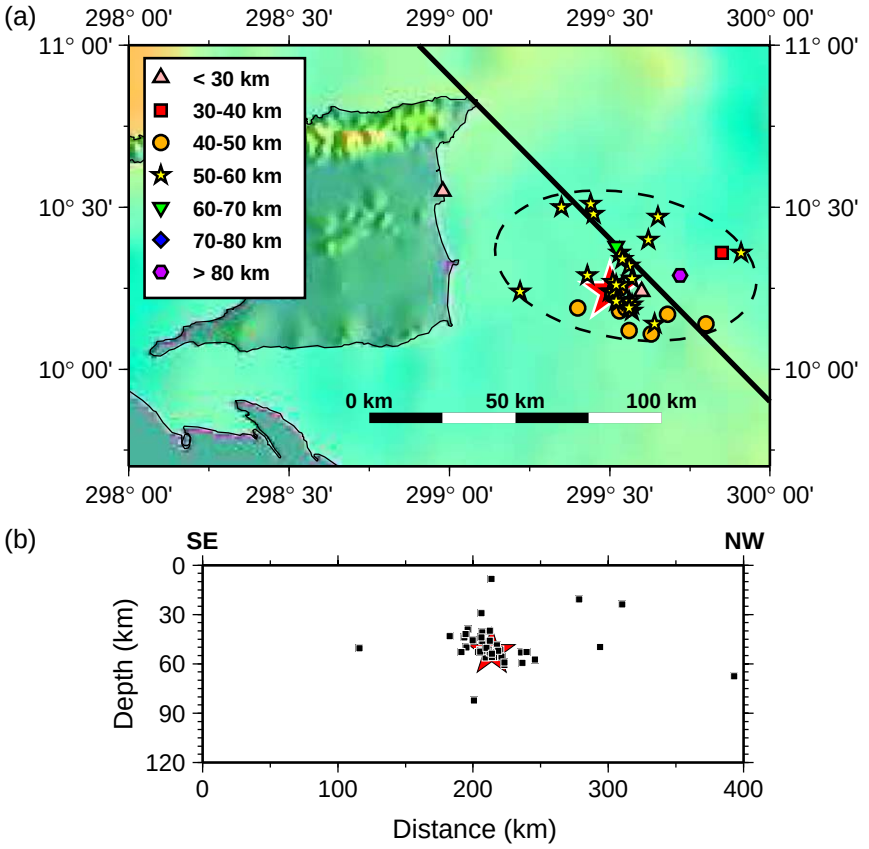

Fig. 6. (a) Geographic depth distribution of relocated seismicity. Note that most relocated aftershocks cluster tightly around the main shock location, and that there is a concentration of events at depths between 40 (circles) and 60 km (stars). The shallower events in this depth range lie almost exclusively south of the deeper events in this cluster. Ellipse encloses all true aftershocks of the March 10, 1988 earthquake. (b) Relocated hypocenters projected onto NW–SE cross section (heavy black line on (a)). Note apparent northward dip of tight tabular zone of aftershocks on section. This figure can be viewed in colour in the web version of this article.

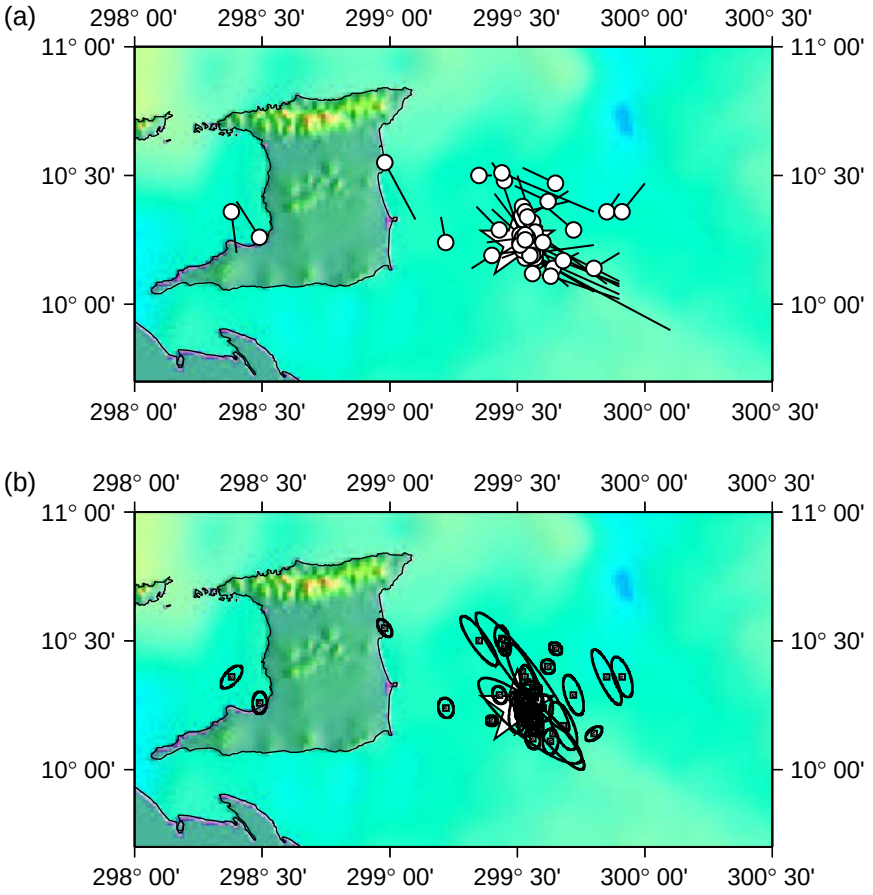

Fig. 7. (a) Relocation vectors of the March 10, 1988 aftershocks. Circles lie at the new epicenters and vectors originate at ISC locations. Note clear tightening of aftershock cluster after relocation and reduction of NW–SE extent of aftershocks apparent in ISC locations. (b) 90% uncertainty ellipses of the relocated epicenters. This figure can be viewed in colour in the web version of this article.

also, but these relocation vectors are shorter than the ones associated with southeastern ISC events. The six events we relocated that were apparently not aftershocks do not reveal systematic epicentral changes, confirming that they are unrelated to the March 10, 1988 earthquake, and indicating that the JHD method does not introduce systematic shifts in location unrelated to the structure of the travel time residuals of the true aftershocks.

The confidence limit ellipses for our relocations (Fig. 7, Table 3) are generally relatively small, indicating good data, well-modeled by the JHD relocation. Several of the aftershocks, however, have large ellipses that trend NW–SE. We infer that this increased uncertainty in our relocations is due to an inhomogeneous station distribution such that most stations lie in the NW quadrant (e.g., North America). The mean latitude difference (Table 2) between ISC and the JHD locations is 11 km for all the true aftershocks, and the mean longitude difference is 17 km. Depth differences vary from a minimum of a few km to around 40 km, maximum, with a mean value for true aftershocks of 14 km (Table 2).

5. Discussion

The aftershocks define a region approximately 80 km in horizontal extent by 30 km in the down-dip direction. The apparent area of the ruptured region is thus on the order of 2400 km^2. Utsu and Seki (1954) report an empirical relationship between fault area, as

Table 3
JHD relocation error ellipses

Date	Time	Azimuth cw from N	Major axis (km)	Minor axis (km)
10 03 88	06:30:18.3	90.29507	8.48751	4.77595
10 03 88	06:33:19.9	104.31847	7.88685	5.16324
10 03 88	23:38:11.5	−25.65458	26.80006	6.72880
11 03 88	00:58:02.0	−13.30415	8.57226	5.30594
11 03 88	06:14:27.5	134.46555	6.22522	4.82402
11 03 88	10:32:32.3	−37.30072	4.61705	8.53336
11 03 88	16:01:02.6	−35.33635	5.04250	4.83058
12 03 88	04:32:05.8	106.52868	5.01769	4.41427
12 03 88	05:24:42.0	−40.57710	40.79583	9.17159
12 03 88	21:37:22.3	−8.17218	11.33722	7.19995
12 03 88	23:00:05.1	−5.87386	10.58451	5.85786
13 03 88	17:00:24.4	−8.37220	9.73630	5.52975
14 03 88	11:53:32.3	−4.53691	11.88664	6.99146
16 03 88	05:47:58.5	91.18320	4.98842	4.32187
16 03 88	14:24:20.4	−31.49771	6.49007	5.71468
17 03 88	11:16:58.2	121.33385	9.53619	7.27636
18 03 88	03:22:59.1	−37.89066	65.36141	11.41741
20 03 88	00:54:15.3	−26.28660	33.33308	8.41134
24 03 88	14:44:49.0	−35.44552	26.28713	6.99789
25 03 88	16:20:42.2	104.53301	5.06953	4.47656
01 04 88	12:59:28.1	−14.94607	8.86408	6.60892
07 04 88	21:47:08.4	2.26624	11.16387	6.79242
14 04 88	07:31:47.9	−12.58673	11.46551	6.12962
22 04 88	10:16:17.7	−8.36108	11.47756	7.10307
28 04 88	22:15:38.3	−12.48960	10.23994	5.75925
30 04 88	21:37:33.9	1.89483	9.73772	6.26073
08 05 88	03:15:41.2	−6.28815	11.57700	6.45241
04 06 88	03:29:50.5	−10.44027	15.18054	6.01284
05 06 88	11:19:24.5	−13.38291	64.49646	14.31505
06 06 88	02:29:08.7	−25.15881	7.99099	5.80604
24 06 88	08:57:49.5	125.49207	6.79335	5.37937
24 06 88	10:27:50.3	42.52728	12.43013	5.88680
24 06 88	10:38:06.0	128.82346	57.02046	15.20819
24 06 88	22:25:50.8	0.64794	11.86887	8.76244
26 06 88	07:03:19.7	129.99709	6.30770	5.49205
02 09 88	08:30:20.6	10.88893	19.97451	9.04249
30 10 88	17:25:17.5	−2.35308	14.33005	8.95729
02 12 88	18:25:16.3	−36.58730	8.97056	4.65759
04 12 88	00:41:00.3	−16.84814	9.22994	6.18532
03 04 89	01:45:46.5	119.28719	37.75191	10.53686
15 04 89	14:26:40.3	111.96667	7.70704	5.64125
24 09 89	16:56:49.2	−19.56080	18.65543	7.34004
27 09 89	23:31:29.2	−18.79999	18.44394	7.14156
09 10 90	21:57:16.0	−22.90673	22.56939	9.06528

defined by aftershock regions, and the MS magnitude of the main shock:

$$\log A = 1.02M_S + 6.0 \quad (1)$$

where A is the aftershock area, in cm^2. Given a main shock M_S of 6.4 (National Earthquake Information Center), the fault area should be only around 340 km^2. However, the aftershock area we calculate for the March 1988 earthquake sequence includes aftershocks that occurred during almost 2 years following the main shock, whereas the Utsu and Seki (1954) method was restricted to inclusion of aftershocks

within only a few days of the main shock. The reason for this restriction is that aftershock regions are often observed to grow rapidly in months and years following an event, indicating an expansion of the ruptured region. This appears to be the case for the March 10, 1988 event. Growth of the ruptured region probably is related to afterslip and creep on a preexisting fault of much larger areal extent than the ruptured region. Given either the long term (2400 km^2) or short term (337 km^2) estimate of the ruptured region, the area of the fault zone probably indicates that this is not the first rupture of this fault, only the first instrumentally observed, implying that future earthquakes in this region are likely to occur along this fault surface.

To determine dip of the apparent fault plane of the relocated earthquakes, we plotted the aftershocks on a vertical plane trending NW–SE (approximately perpendicular to the strikes of the CMT nodal planes, see Fig. 5) and fit a line to the points. We excluded the six events that were clearly not aftershocks in the fitting. The regression yielded a rather precisely defined plane, dipping 34° to the NW (Fig. 8). This dip is in excellent agreement with the Harvard CMT focal mechanism, which has one nodal plane dipping 38°N and striking ENE. Thus, we infer that this north-dipping nodal plane is the fault plane of March 10, 1988 main shock.

Based on our analysis of stress modes related to subduction and slab detachment or lithospheric flexure (see Introduction), and given the depth of the main shock, 53 km, this result clearly is not consistent with a flexural origin of the stresses leading to the seismicity. Seismicity resulting from lithospheric flexure should occur at shallow depths in the lithosphere and should occur on fault planes that dip steeply away from the subduction trench. The March 10, 1988 earthquake and aftershocks, in contrast, occurred at sub-crustal depths, and the main shock fault plane dips shallowly towards the NW, towards the subduction zone. Thus, it is more likely that the March 10, 1988 sequence was caused by subduction and slab detachment.

The compression axis of the main shock focal mechanism plunges nearly vertically, and the tension axis trends NW and plunges shallowly. We interpret the fact that the tension axis in lithosphere at 50 km depth plunges in the direction of local slab dip as indicating that slab pull is an important source of

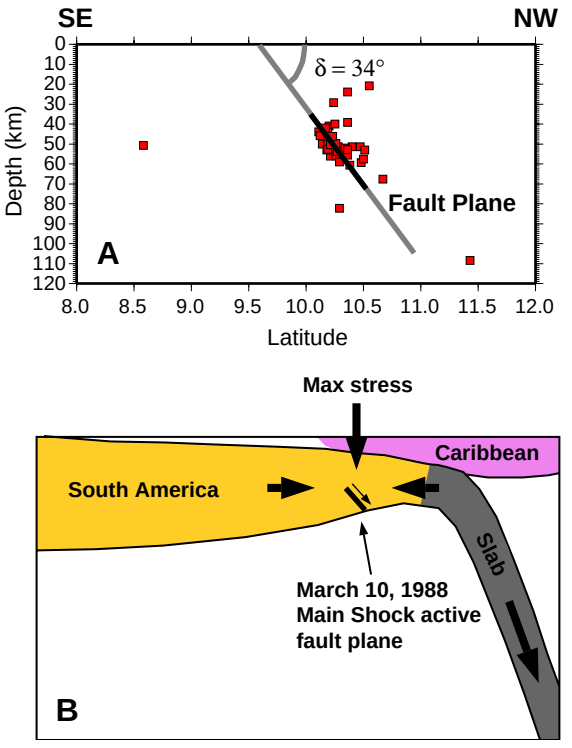

Fig. 8. Top—vertical NW–SE section through the aftershock hypocenters. Line is best fit to true aftershocks. Dip of the fault plane as defined by the aftershocks is around 34°NW. Bottom—schematic cross section of subducting South American continental lithosphere showing our interpretation of the March 10, 1988 earthquake. Heavy arrows indicate max and min compressive stresses indicated by the earthquake focal mechanism. This figure can be viewed in colour in the web version of this article.

stress in this region of likely slab termination and tearing (e.g., Yoshioka and Wortel, 1995). The fact that the compression axis is nearly vertical is very unusual for an earthquake of this depth not in a subducted slab. Our interpretation of this earthquake and of the significance of its active fault plane is shown in Fig. 8. We relate the main shock to a combination of vertical loading on downwarped South American lithosphere due to overriding by the Caribbean plate, and to slab pull on the subducted and detaching oceanic portion of the South American plate (Russo and Speed, 1992, 1994; Russo et al., 1996; VanDecar et al., 2003). Thus, we account for the strike of the active fault plane (parallel to the subduction zone to the NW),and for the shallow northward dip of the fault plane (maximum stress is close to vertical and shear occurs on a plane dipping shallowly). Our

interpretation also accounts for the generally unexpected depth of normal faulting here: the rupture occurred in South American continental mantle lithosphere that has been downwarped due to the subduction and overriding by the Caribbean plate. In combination with the negative buoyancy of the old (late Cretaceous) oceanic slab portion of South America, concentrated at the locus of current detachment beneath the Gulf of Paria and adjacent Trinidad, resultant stresses on the deep lithosphere are strongly tensional (Yoshioka and Wortel, 1995).

6. Conclusions

Our study resulted in a better understanding of the tectonics of the region east of Trinidad, and suggests possible causes of the March 10, 1988, main shock. The hypocenters of the relocated aftershocks lead to a clear determination of the fault plane of the March 10 earthquake. The fault plane we find is consistent with the Harvard CMT mechanism for the main shock, and defines a plane that strikes ENE and dips around 35°NW. The fault area is 30 km (depth) by 80 km (EW), larger than one would expect given the magnitude of the main shock and resultant short term estimates of fault rupture area. The size of the ruptured region indicates that the fault most likely pre-existed this rupturing episode, as more active faults tend to be larger in area. This inference implies recurrence of this type of event in the study region. The unusual depth and placement of the normal-faulting main shock appears to result from a combination of vertical loading of South American lithosphere and concentrated slab pull on continental South American lithosphere as detaching subducted oceanic South American lithosphere sinks beneath the Caribbean plate. The combined effect of vertical maximum stress and near horizontal slab pull (actually a minimum compressive stress) on the lithosphere causes normal faulting at unusual depth in the unsubducted lithosphere.

Acknowledgments

J. Marshall was supported by an Undergraduate Research Grant from Northwestern University. We used GMT (Wessel and Smith, 1991, 1995) to plot figures in this paper. We thank the two anonymous reviewer.

References

Avé Lallement, H.G., 1997. Transpression, displacement partitioning, and exhumation in the eastern Caribbean/South American plate boundary zone. Tectonics 16, 272–289.

Dewey, J.W., 1972. Seismicity and tectonics of western Venezuela. Bull. Seismol. Soc. Am. 62, 1711–1751.

Douglas, A., 1967. Joint epicentre determination. Nature 215, 47–48.

Dziewonski, A.M., Ekström, G., Woodhouse, J.H., Zwart, G., 1989. Centroid-moment tensor solutions for January–March 1988. Phys. Earth Planet. Inter. 54, 22–31.

McCann, W.R., Sykes, L.R., 1984. Subduction of aseismic ridges beneath the Caribbean plate: implications for the tectonics and seismic potential of the northeastern Caribbean. J. Geophys. Res. 89, 4493–4519.

Mendoza, C., Hartzell, S.H., 1988. Aftershock patterns and main shock faulting. Bull. Seismol. Soc. Am. 78, 1438–1449.

Molnar, P., Sykes, L., 1969. Tectonics of the Caribbean and Middle America regions from focal mechanisms and seismicity. Geol. Soc. Amer. Bull. 80, 1639–1684.

Parnaud, F., Gou, Y., Pascual, J.-C., Truskowski, I., Gallango, O., Passalacqua, H., Roure, F., 1995. Petroleum geology of the central part of the eastern Venezuelan Basin. In: Tankard, A.J., Suárez, R., Welsink, H.J. (Eds.), Petroleum Basins of South America, Amer. Assoc. Petrol. Geo. Mem., vol. 62, pp. 741–756.

Passalacqua, H., Fernandez, F., Gou, Y., Roure, F., 1995. Crustal architecture and train partitioning in the eastern Venezuelan ranges. In: Tankard, A.J., Suárez, R., Welsink, H.J. (Eds.), Petroleum Basins of South America, Amer. Assoc. Petrol. Geo. Mem., vol. 62, pp. 741–756.

Perez, O.J., Aggarwal, Y.P., 1981. Present-day tectonics of the southeastern Caribbean and northeastern Venezuela. J. Geophys. Res. 86, 10791–10804.

Perez, O.J., Bilham, R., Bendick, R., Velandia, J.R., Hernandez, N., Moncayo, C., Hoyer, M., Kozuch, M., 2001. Velocity field across the southern Caribbean plate boundary and estimates of Caribbean/South American plate motion using GPS geodesy 1994–2000. Geophys. Res. Lett. 28, 2987–2990.

Rial, J., 1978. The Caracas, Venezuela, earthquake of 30 July 1967: a multiple source event. J. Geophys. Res. 83, 5405–5414.

Rossi, T., Stephan, J.-F., Blanchet, R., Hernandez, G., 1987. Étude géologique de la Serranía del Interior Oriental (Venezuela) sur le transect Cariaco-Maturin. Rev. Inst. Fr. Pét. 42, 3–30.

Roure, F., Carnevali, J.O., Gou, Y., Subieta, T., 1994. Geometry and kinematics of the north Monagas thrust belt (Venezuela). Mar. Pet. Geol. 11, 347–362.

Russo, R.M., Speed, R.C., 1992. Oblique collision and tectonic wedging of the South American continent and Caribbean terranes. Geology 20, 447–450.

Russo, R.M., Speed, R.C., 1994. Spectral analysis of gravity anomalies and the architecture of tectonic wedging, NE Venezuela and Trinidad. Tectonics 13, 613–622.

Russo, R.M., Okal, E.A., Rowley, K.C., 1992. Historical seismicity of the southeastern Caribbean and tectonic implications. Pure Appl. Geophys. 139, 87–120.

Russo, R.M., Speed, R.C., Okal, E.A., Shepherd, J.B., Rowley, K.C., 1993. Seismicity and tectonics of the southeastern Caribbean. J. Geophys. Res. 98, 14299–14319.

Russo, R.M., Silver, P.G., Franke, M., Ambeh, W.B., James, D.E., 1996. Shear-wave splitting in northeast Venezuela, Trinidad, and the eastern Caribbean. Phys. Earth Planet. Inter. 95, 251–275.

Sandwell, D.T., Smith, W.H.F., 1997. Marine gravity anomaly from Geosat and ERS-1 satellite altimetry. J. Geophys. Res. 102, 10039–10054.

Shepherd, J.B., Aspinall, W.P., 1983. Seismicity and earthquake hazard in Trinidad and Tobago, West Indies. Earthquake Eng. Struct. Dyn. 2, 229–250.

Speed, R.C., 1985. Cenozoic collision of the Lesser Antilles Arc and continental South America and the origin of the El Pilar Fault. Tectonics 4, 41–69.

Stein, R.S., Barrientos, S.E., 1985. Planar high-angle faulting in the basin and range: geodetic analysis of the 1983 Borah Peak, Idaho, earthquake. J. Geophys. Res. 90, 11355–11366.

Stein, S., Engeln, J., Wiens, D., Fujita, K., Speed, R., 1982. Subduction seismicity and tectonics in the Lesser Antilles Arc. J. Geophys. Res. 87, 8642–8664.

Stein, S., Engeln, J., Wiens, D., Speed, R., Fujita, K., 1983. Slow subduction of old lithosphere in the Lesser Antilles. Tectonophysics 99, 139–148.

Utsu, T., Seki, A., 1954. A relation between the area of aftershock region and the energy of main shock. J. Seismol. Soc. Jpn. 7, 233–240.

VanDecar, J.C., Russo, R.M., James, D.E., Ambeh, W.B., Franke, M., 2003. Aseismic continuation of the Lesser Antilles slab beneath northeastern Venezuela. J. Geophys. Res. 108, doi:10.1029/2001JB000884.

van der Hilst, R., 1990. Tomography with P, PP and pP delay-time data and the three-dimensional mantle structure below the Caribbean region. PhD thesis, University of Utrecht, 250 p.

Wadge, G., Shepherd, J.B., 1984. Segmentation of the Lesser Antilles subduction zone. Earth Planet. Sci. Lett. 71, 297–304.

Weber, J.C., Dixon, T.H., DeMets, C., Ambeh, W.B., Jansma, P., Mattioli, G., Saleh, J., Sella, G., Bilham, R., Perez, O., 2001. GPS estimates of relative motion between the Caribbean and South American plates, and geologic implications for Trinidad and Venezuela. Geology 29, 75–78.

Wessel, P., Smith, W.H.F., 1991. Free software helps map and display data. Eos, Trans.-Am. Geophys. Union 72, 441–446.

Wessel, P., Smith, W.H.F., 1995. New version of the generic mapping tools released. Eos, Trans.-Am. Geophys. Union 76, 329.

Wortel, M.J.R., Spakman, W., 2000. Subduction and slab detachment in the Mediterranean–Carpathian region. Science 290, 1910–1917.

Yoshioka, S., Wortel, M.J.R., 1995. Three-dimensional numerical modeling of detachment of subducted lithosphere. J. Geophys. Res. 100, 20223–20244.